

Solvothermal vapor annealing setup for thin film treatment

A compact design with in situ solvent vapor concentration probe

Ariaee, Sina; Jakobsen, Bo; Pedersen, Ib Høst; Rasmussen, Torben Steen; Posselt, Dorthe

Published in:
AIP Advances

DOI:
[10.1063/5.0152666](https://doi.org/10.1063/5.0152666)

Publication date:
2023

Document Version
Publisher's PDF, also known as Version of record

Citation for published version (APA):

Ariaee, S., Jakobsen, B., Pedersen, I. H., Rasmussen, T. S., & Posselt, D. (2023). Solvothermal vapor annealing setup for thin film treatment: A compact design with *in situ* solvent vapor concentration probe. *AIP Advances*, 13(6), Article 065226. <https://doi.org/10.1063/5.0152666>

General rights

Copyright and moral rights for the publications made accessible in the public portal are retained by the authors and/or other copyright owners and it is a condition of accessing publications that users recognise and abide by the legal requirements associated with these rights.


- Users may download and print one copy of any publication from the public portal for the purpose of private study or research.
- You may not further distribute the material or use it for any profit-making activity or commercial gain.
- You may freely distribute the URL identifying the publication in the public portal.

Take down policy

If you believe that this document breaches copyright please contact rucforsk@kb.dk providing details, and we will remove access to the work immediately and investigate your claim.

RESEARCH ARTICLE | JUNE 26 2023

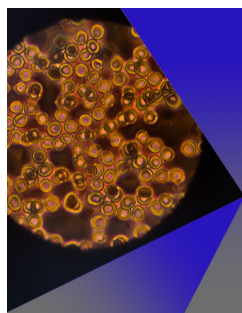
Solvothermal vapor annealing setup for thin film treatment: A compact design with *in situ* solvent vapor concentration probe ^{EP}

Sina Ariaee ^{ID} ; Bo Jakobsen ^{ID} ; Ib Høst Pedersen; Torben Steen Rasmussen; Dorthe Posselt ^{ID} 

AIP Advances 13, 065226 (2023)

<https://doi.org/10.1063/5.0152666>View
OnlineExport
Citation

CrossMark

**AIP Advances**Special Topic: Medical Applications
of Nanoscience and Nanotechnology**Submit Today!**

Solvothermal vapor annealing setup for thin film treatment: A compact design with *in situ* solvent vapor concentration probe

Cite as: AIP Advances 13, 065226 (2023); doi: 10.1063/5.0152666

Submitted: 31 March 2023 • Accepted: 2 June 2023 •

Published Online: 26 June 2023



Sina Ariaee,  Bo Jakobsen,  Ib Høst Pedersen, Torben Steen Rasmussen, and Dorte Posselt^{a)} 

AFFILIATIONS

IMFUA, Department of Science and Environment, Roskilde University, P.O. Box 260, 4000 Roskilde, Denmark

^{a)} Author to whom correspondence should be addressed: Dorte@ruc.dk

ABSTRACT

A compact setup for *in situ* solvothermal vapor annealing of thin polymer films in the temperature range from room temperature to 70 °C is presented. The design is optimized to avoid solvent condensation in tubes and other components. The setup consists of a chamber, a gas delivery system, a commercial film-thickness measuring device, and a solvent vapor concentration sensor. The chamber is equipped with heaters and thermometers and is thermally insulated. It has windows to allow for penetration of x-rays together with a sample table with a gas distributor to ensure homogeneous swelling of the polymer film. The computer-controlled gas delivery system has two different components, which can be used separately or in parallel (for mixed gas solvent annealing): (a) mass flow controllers and a bubbler system and (b) a commercial “controlled evaporation and mixing” system. The film-swelling ratio is determined *in situ* using optical reflectometry, and the solvent concentration in the exhaust gas is continuously monitored by UV-absorption. Test results are presented where the setup is used for swelling of ~100 nm thick polystyrene and polyisoprene homopolymer films with toluene and acetone, respectively.

© 2023 Author(s). All article content, except where otherwise noted, is licensed under a Creative Commons Attribution (CC BY) license (<http://creativecommons.org/licenses/by/4.0/>). <https://doi.org/10.1063/5.0152666>

I. INTRODUCTION

Polymer thin films swell when taking up solvent vapor, the degree of swelling depending on the specific solvent–polymer interaction.¹ The swelling behavior of polymers, in general, is of fundamental interest in order to understand polymer–solvent dynamics.^{2,3} An important class of materials in nanotechnology are block copolymers (BCPs), i.e., chemically different polymers bound together with covalent bonds and forming different architectures from linear to highly branched.⁴ BCPs are of potential use in various applications, including nanolithography,^{5,6} nano-patterning and templating,^{7,8} semi-conductors,⁹ membranes,¹⁰ solar-cells,¹¹ and ion exchange.¹²

Solvent Vapor Annealing (SVA) is a highly versatile method used to increase long-range order in BCPs with nanoscale ordered morphology; to heal defects from, e.g., spin-coating or other sample preparation methods; to alter the orientation of microdomains; and to change the morphology in special cases.¹³ SVA as a practical means for annealing in BCP processing was first introduced in

1995¹⁴ and rapidly gained a place as a versatile and gentle alternative to the more conventional thermal annealing method.^{15,16} The solvent–polymer interaction in SVA increases chain mobility and lowers the effective glass transition temperature, T_g , of the polymers.¹⁷ SVA can also reduce interactions between polymer chains and thin film substrates.^{18–20} In addition, several research groups have employed SVA in the guided self-assembly of BCPs.^{6,21–23}

SVA setups have evolved from simple liquid reservoir chambers (e.g., a sealed jar with a sample stage and a liquid solvent reservoir inside) with annealing time as the only control variable.^{15,24} More sophisticated SVA setups with input/output tubing systems came next in order to adjust the solvent removal rate from the container.⁹ Later, SVA instrumentation expanded to the development of annealing setups with automated flow controllers to produce a controlled solvent vapor atmosphere.^{25–28} In this regard, Hoang *et al.* reported a SVA setup coupled with an *in situ* fluorescence microscopy probe, allowing for single particle tracking.¹ Efremov *et al.* introduced an environmental SVA chamber equipped with an *in situ*

spectroscopic ellipsometer.²⁹ Jin *et al.* expanded their SVA chamber with a solvent vapor feedback loop designed in order to attain a constant film swelling degree automatically.⁷ Nelson *et al.* designed their SVA setup with pneumatic valves and the capacity of maintaining the SVA time in the millisecond range.²⁵ In order to decrease the annealing time from hours to minutes, in some instruments, the possibility of performing SVA at somewhat elevated temperatures has been implemented, and this method has been labeled solvothermal vapor annealing (STVA).^{30–34}

An important point to address when designing a STVA chamber is the elimination of solvent vapor condensation in tubing and restricted access places.^{35–40} The starting point for the state-of-the-art design of a STVA setup presented in this paper is the setup developed by our collaborators at TU-Munich.^{13,40} In this new design, tubing is minimized by placing the liquid solvent bubbler reservoir in direct contact with the metal body of the STVA chamber. This way, temperature regulation of the whole STVA chamber, including bubbler systems, is simplified and condensation problems minimized. In addition, the setup is equipped with a home-made UV-absorption sensor, allowing for real-time solvent vapor concentration (SVC) monitoring of the exhaust gas from the STVA chamber. The setup has two computer-controlled solvent vapor delivery systems based on (a) mass flow controllers (MFCs) and a bubbler solvent reservoir and (b) a commercial unit for controlled evaporation and mixing (CEM) of liquid solvent and carrier gas before the resulting gas mixture at specified temperature, humidity, and flow rate is let into the STVA chamber. The versatility, compact size, and low weight (~2 kg) give the setup the capacity to be used for *in situ* studies at synchrotron beamlines [e.g., small-angle x-ray scattering (SAXS) or grazing incidence small-angle x-ray scattering (GISAXS)] and for in-house studies. The STVA chamber in the current setup is designed for surface studies, i.e., samples (thin films) prepared on, e.g., Si-wafers are placed on a sample table in the chamber, allowing x-rays to pass through a suitable window and hit the sample surface at very low incident angles ($\sim 0.1^\circ - 0.2^\circ$), while the reflected beam can pass through a similar window (GISAXS). This setup is easily adapted to x-ray transmission measurements (SAXS). For surface studies, the chamber is equipped with an *in situ* thickness monitor.

In this paper, design and technical considerations when constructing the STVA setup are presented together with suitable performance tests of the setup. The full setup is tested on solvent vapor swelling of thin homopolymer films spin coated onto silicon wafers [polystyrene (PS) and polyisoprene (PI)] and swollen with toluene and acetone, respectively, where the chamber gas humidity is monitored by the SVC probe and the swelling of the sample is followed *in situ* using white light reflectometry to measure the film thickness changes as a function of time.

II. COMPACT SOLVOTHERMAL VAPOR ANNEALING SETUP

The custom-made STVA setup is composed of four distinct components: (1) STVA chamber, (2) solvent vapor delivery system, (3) a gauge for *in situ* SVC measurements, and (4) a commercial *in situ* optical film thickness monitoring (OFTM) probe.

A. STVA chamber

Figure 1 shows both photos and schematic drawings of the STVA chamber seen from different viewpoints. In Fig. S1 of the supplementary material, photos show the STVA setup when mounted at a GISAXS beam-line.

The STVA chamber (Fig. 1) is constructed from aluminum to be inert against solvent vapor. The chamber has a volume of $\sim 375 \text{ cm}^3$ and is equipped with two Kapton windows (thickness $\sim 0.13 \text{ mm}$) with an acceptable low x-ray absorption to allow for, e.g., GISAXS and SAXS measurements. Two resistive heating elements (Polyimide Thermo-foil Heater, 28 V, 12 W, from Minco Co.) are connected to the sidewalls. In addition, two thermometers (PT100) are mounted and coupled with a temperature controller (from Omron Co.) for temperature regulating. The thermometers are placed sufficiently close to the heating elements to comfort the Proportional-Integral-Derivatives (PID) temperature controller algorithm. The bubbler, i.e., the liquid solvent reservoir, is mounted at the backside of the STVA chamber in thermal contact with the chamber sidewall, promoting thermal equilibrium with the whole chamber. It is fabricated from the stainless steel plate to be chemically inert against liquid solvents, corrosion resistant, and easy to maintain. A mixing box for mixing of solvent vapor and dry N_2 gas is connected between the bubbler and the chamber. All tubing is 1/8 in. stainless steel tubes for maximal temperature stability. The aluminum sample stage is mounted inside the chamber ($\sim 35 \times 35 \times 20 \text{ mm}^3$) and can be equipped with a PT100 thermometer. For a spatially homogeneous vapor delivery to the sample, a gas distributor is used, which is made of a stainless steel tube bent around the sample stage and containing two holes per side — i.e., in total eight holes. It is important to ensure a homogeneous distribution of solvent vapor around the sample in order to avoid any time lag across the $\sim 15 \text{ mm}$ wide sample, as was observed while using a STVA setup with a solvent vapor diffuser placed at one side of the film.⁴⁰ Samples are loaded into the chamber from a top opening with a lid and placed onto the sample stage. The lid is equipped with a window and a holder for the optics and the fiber of the OFTM probe, allowing these elements to be separated from the relatively harsh atmosphere in the chamber (see Figs. S2 and S3). The lid is tightened to the chamber opening with thumb screws and a swelling resistant O-ring (different types have been tested, including Viton Ltd. and DuPont Kalrez; the latter is the best suitable for this use). The walls of the sample chamber are held together with bored-through screws and a thermally conductive epoxy sealant (Loctite STYCAST 2850 ft, Henkel) to assure a good seal. Thermal insulation is done by covering the STVA chamber with Vekaplan-S rigid PVC foam insulation sheets utilizing plastic screws.

B. Solvent vapor delivery system

The solvent vapor delivery unit is composed of two distinctive sub-systems for producing solvent vapor, which can be used separately or simultaneously: (i) a combination of MFCs and a bubbler and (ii) a combination of MFCs and a CEM system (both from Bronkhorst High-Tech B.V.). Figure 2 represents a schematic drawing of the solvent vapor delivery system and shows how the different parts are connected.

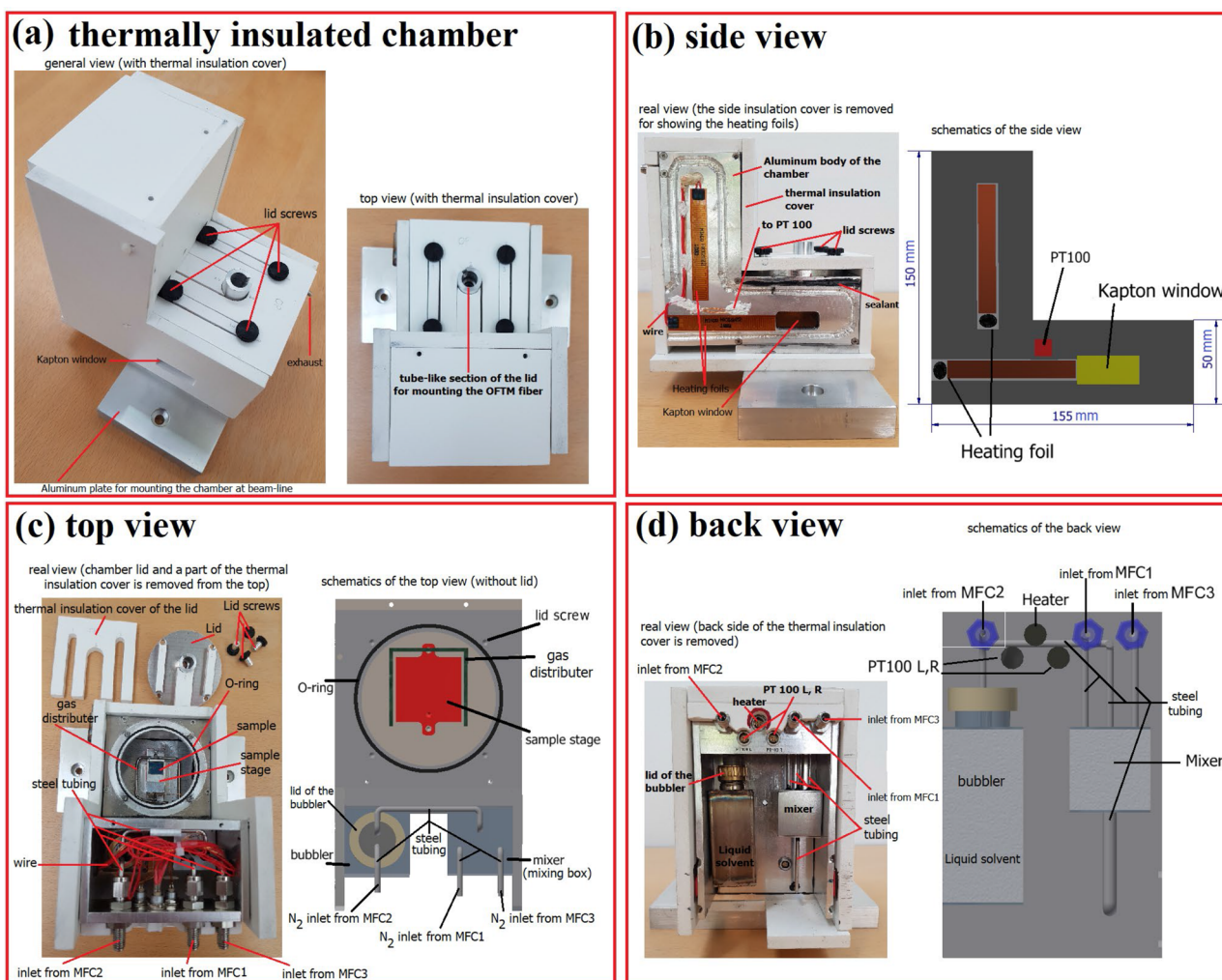


FIG. 1. Photos and schematics of the STVA chamber from different viewpoints. (a) Photos of the chamber with the thermal insulation cover and the aluminum plate used for mounting it at the beam-line. (b) Side view of the chamber exhibiting the heating foils, thermometer, and Kapton window. (c) Top view of the chamber after removing the chamber lid presenting the sample stage, the gas distributor, gas inlets from mass flow controllers, and a thin film sample placed on the sample stage. (d) Backside view of the chamber showing the bubbler, mixer, steel tubing, and heater outlet. PT100 L and PT100 R point to the platinum thermometers at the left-hand side and right-hand side of the chamber, respectively.

When using the combination of MFCs and a bubbler [see Fig. S2(a)], initial dry N_2 gas flow ($\sim 5\text{--}8$ bars) is split into three parallel flows and passes through three MFCs with the flow capacity of 400, 200, and 200 sccm, respectively. The 400 sccm channel is designated to transfer dry gas and is directly connected to the mixer to be used for solvent vapor dilution and for final film drying. One of the 200 sccm gas flows is connected to the bubbler as carrier gas to be saturated with solvent vapor in the bubbler and then transferred as wet gas to the mixer. The other 200 sccm channel can be used with CEM solvent vapor delivery either alone or for studies of mixed solvent annealing. The wet gas mixture is then transferred to the STVA chamber utilizing the gas distributor. An essential feature of the design using a bubbler vapor delivery system is that

the compact all-metal design allows all parts to be in good thermal contact, which reduces the risk of solvent condensation in chamber components.

In cases where we use the combination of MFCs and the controlled evaporation and mixing device (CEM Evaporator W-102 A from Bronkhorst) [see Fig. S2(b)], the gas/liquid flow is rather different. The central feature of the CEM system is control of the mixture of gas and liquid to achieve a specific degree of solvent vapor concentration at a desired temperature and gas flow. The CEM is supported by thermodynamic software (FLUIDAT, from Bronkhorst) to calculate the liquid flow into the mixing unit to be used for a desired temperature, solvent vapor concentration, and gas flow into the experimental chamber. In contrast, a fundamental

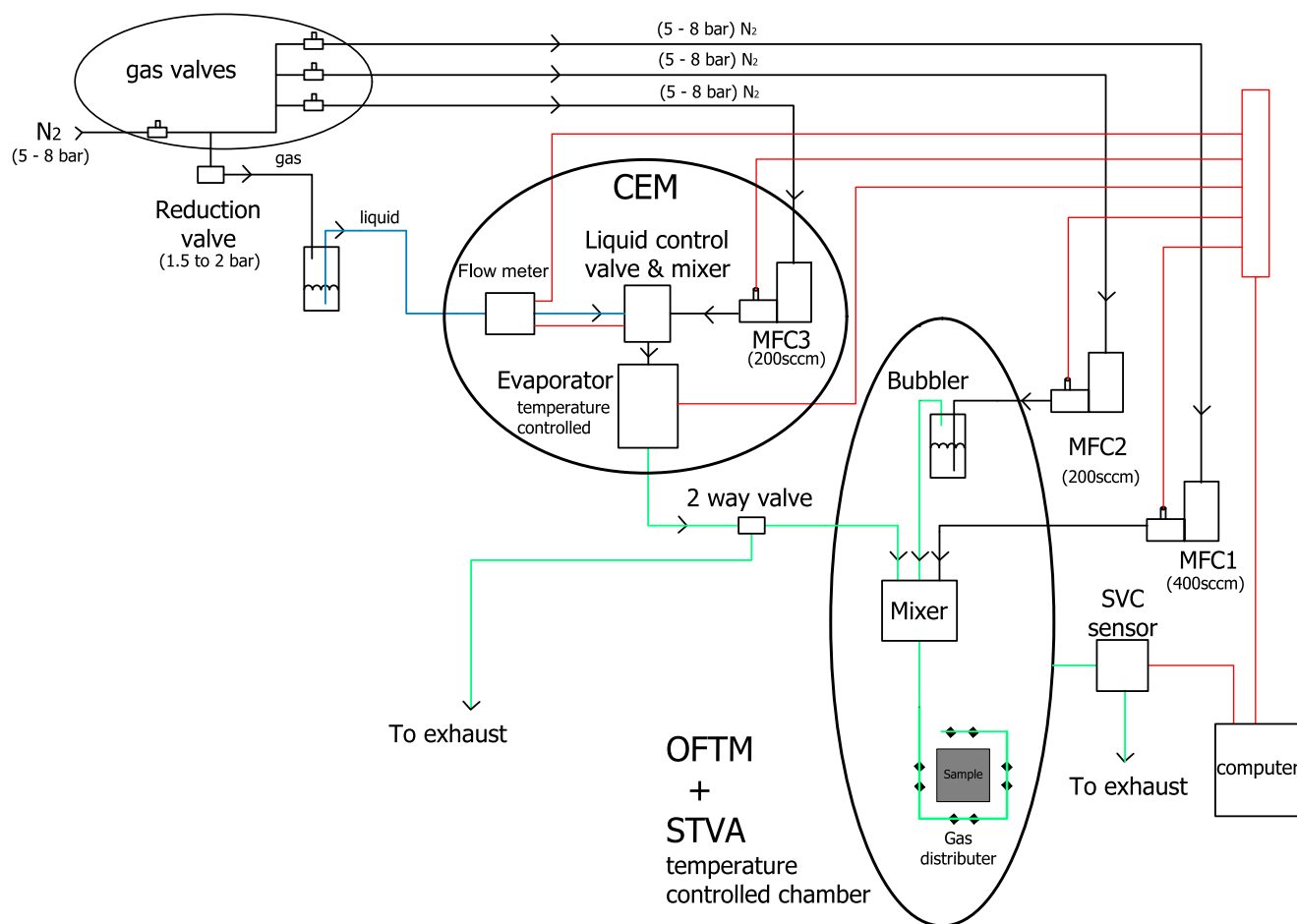


FIG. 2. Schematic drawing of the two solvent vapor delivery systems and how they are connected to the STVA chamber. Schematic drawings of the data cables (red), the tubes for solvent vapor (i.e., wet carrier gas) transfer (green), the tubes for the liquid solvent transfer (blue), and the tubes for carrying N₂, i.e., dry gas (black).

assumption using the bubbler system is that the N₂ bubbles are saturated with organic solvent vapor when the bubbles are passing through the liquid solvent in the bubbler, which might be a problem when the bubbler is emptying and the path length through solvent is getting short. Using the CEM, a steady and controllable liquid solvent stream is achieved by pressurizing a 250 ml Borosilicate glass liquid solvent container (Duran pressure plus + for safely maintaining pressures up to ~1.5 bars) with nitrogen gas at ~1 bar (maintained by a Festo MS4-LR-1 pressure gauge) and extracting the pure liquid solvent from this reservoir. The solvent stream is transferred to the Coriolis liquid flowmeter (20 g/h mini CORI-FLOW, which is part of the Bronkhorst CEM system), which measures and controls the liquid flow. The control of the flow is done using the “liquid control valve,” which is integrated into the CEM unit utilizing a PID-controlled analog signal from the CORI-FLOW to the valve. The valve is of a proprietary design and able to control the flow rate based on the input voltage. The set point liquid flow is calculated using an online software (FLUIDAT, from Bronkhorst), which conveniently calculates the required liquid flow

for a given solvent, final temperature, gas flow, and required solvent concentration.

The liquid solvent flow is mixed with the gas flow (obtained from a 200 sccm MFC channel) in the “liquid control valve and mixer” unit and transferred to the evaporation chamber of the CEM. The temperature of the evaporation chamber is controlled to allow for obtaining vapor concentrations at different temperatures. The evaporation chamber temperature is normally set to the same temperature as the temperature of the STVA chamber (or in some cases, a few degrees higher, to minimize condensation in the tubes). Finally, gas with a given solvent concentration and temperature is delivered to the STVA chamber at a given flow rate.

In solvent vapor delivery sub-systems, chemical resistant hoses (Nylon OD = 1/8 in.), flangeless fittings, and valves (both from IDEX Health & Science LLC) are used for tubing where flexibility is needed in addition to chemical resistivity. For other tubing, 316L-SS Swagelok valves, fittings, and tubing of suitable sizes (all from Fitok Co.) are used. All flows are controlled with readout and control programs (Bronkhorst High-Tech B.V.), allowing for manual and

programmed control. The two solvent vapor delivery sub-systems are designed in a way to make the STVA setup capable of fast drying (quenching) of thin films by shutting down the solvent vapor channels and purging dry N₂ through the chamber. This is of importance for preserving a desired morphology obtained, e.g., during solvent vapor annealing of a block copolymer thin film.^{25,30,40}

C. *In situ* optical film thickness measurement

Monitoring the time-dependent swelling and de-swelling (drying) of thin films during the STVA process is of crucial importance both to have an *in situ* control and monitoring of the setup performance and, more fundamentally, to obtain a better understanding of the interaction between solvent and film material. As an example, *in situ* thickness monitoring has proved to be an important tool for monitoring the swelling process during studies on morphological changes in block copolymer thin films during STVA.⁴⁰ The swelling ratio, *SR*, is calculated as $SR = h(t)/h_0$, where h_0 is the initial film thickness and $h(t)$ is the actual, time-dependent, film thickness. For this purpose, *in situ* ellipsometry²⁹ or *in situ* optical reflectometry measurements^{25,30,40} are possible options. Monitoring the swelling ratio gives insights on the STVA protocol efficiency and, e.g., the approach of the annealed system to thermodynamic equilibrium, polymer chain dynamics^{18,27,41} and interfacial interactions with the substrate.^{42,43}

In optical reflectometry, the film thickness can be determined by analyzing the measured wavelength dependent reflectivity. A model is fitted to the measured film reflectance, $R_{film}(\lambda)$, with the film thickness as one of the fitting parameters. For a given refractive index of the film material (n_{film}) and the substrate ($n_{substrate}$), the film reflectance is calculated as

$$R_{film}(\lambda) = R_{sub}(\lambda) \frac{M(\lambda) - D(\lambda)}{R(\lambda) - D(\lambda)}, \quad (1)$$

where R_{sub} is the optical reflectance of the bare substrate before coating with the film for which table values are used. $M(\lambda)$ is the measured spectrum from the coated substrate, i.e., the thin film. $D(\lambda)$ is the dark spectrum, which is measured by attaching a patch of dark colored cloth with a rough and non-reflecting surface under the measuring probe in order to obtain the internal stray reflectance of the probe. $R(\lambda)$ is the reference spectrum, which is obtained from the bare substrate prior to coating. For the setup presented in this paper, a commercial general-purpose OFTM setup (NanoCalc-XR Ocean Optics Ltd.) with analysis software, including a library of material constants, e.g., refractive indices, for relevant materials, is used.

The setup is composed of three main parts (Fig. S3):

- (1) An external halogen light source (HL-2000-HP-FHSA) with light emission in the range $\lambda = 400 - 850$ nm. A strong external source is substituting the weaker integrated NanoCalc source for the setup presented to compensate for light absorption in lid window and fiber optics.
- (2) A UV-visible light spectrophotometer measuring the reflected light intensity in the range $\lambda = 400 - 1050$ nm with 0.1 nm optical resolution with the incident light normal to the sample surface.
- (3) A long (~1 m) UV-optical fiber (NC-7UV-VIS200-2) with flexible metal jacketing. The fiber and optics must be protected from long-term solvent vapor exposure. The fiber is

thus mounted in a holder in the chamber lid with optics (COL-UV-6.35) and an MgF₂ coated sapphire window from Edmund Optics separating the experimental chamber from the optics. The chamber lid is sealed against solvent vapor leakage with an O-ring (from DuPont Kalrez), which is resistant to solvent vapor.

The external lamp and the additional optics are necessary to ensure a reasonable amount of reflected signal both because of the chamber lid window and because the distance from the OFTM fiber to film surface is ~15–20 mm in the STVA chamber, which is larger than the distance recommended by the manufacturer for the original design (~5 mm).

The commercial software (NanoCalc NC-10n) is used for *in situ* tracking of the film thickness. The software includes a library of material constants and reflectance models for standard substrates and films. The user selects the average refractive index of the film (n_{film}) with unknown thickness, which is coated on a given substrate with a known refractive index ($n_{substrate}$) and infinite thickness. In most cases, it is relevant to include a SiO_x layer on top of the substrate — a typical example being a 1–2 nm thick SiO₂ layer with refractive index 1.46 (see Fig. S4). Additional software was written in order to enable the OFTM system to store and plot measured raw intensity curves for off-line re-analysis purposes (see Fig. 4 and Fig. S5 and Table S1 of the supplementary material). For *in situ* tracking of the film thickness, spectral reflectance data are recorded at typical 10 s time intervals with an integration time of 75 – 85 ms. Experimental data are modeled over a spectral range of 400 – 850 nm with a multi-layer model (typical Si-substrate + Si-oxide layer + thin film).

D. *In situ* solvent vapor concentration sensor

In contrast to the dry N₂ carrier gas, solvent molecules with π bonding (e.g., toluene and acetone) absorb in the UV range (see Fig. S6). Hence, absorption of UV light in the exhaust vapor is used to measure the solvent vapor concentration. Figure 3 represents a schematic overview of the components of the *in situ* SVC sensor.

The sensor for SVC monitoring consists of an inlet tube introducing the solvent vapor flowing out of the STVA chamber to the SVC sensing cell (i.e., gas cell in the schematic in Fig. 3). The gas cell sits between a mercury lamp (~5 mW, Philips G4T5, 4 W) providing 254 nm UV radiation and a quartz-lens (D10*5 mm quartz hemisphere lens) coupled with a UV photodiode (SGLUX, SG01S-18). The output from another photodiode in direct contact with the lamp is used to stabilize the output from the lamp. The transmittance, T , of the solvent gas is determined by monitoring the ratio between the intensity transmitted through the exhaust gas from the STVA chamber (I) and the incident UV light intensity (I_0). The controller circuit reports I to the controller computer at 20 ms time intervals, where $I = 100$ corresponds to dry gas and no transmitted light corresponds to $I = 0$. The output is converted to absorbance, A , according to

$$A = -\log_{10} T = -\log_{10} \frac{I}{I_0}. \quad (2)$$

The absorbance is given by the Lambert–Beer law,^{44,45}

$$A = \epsilon lc, \quad (3)$$

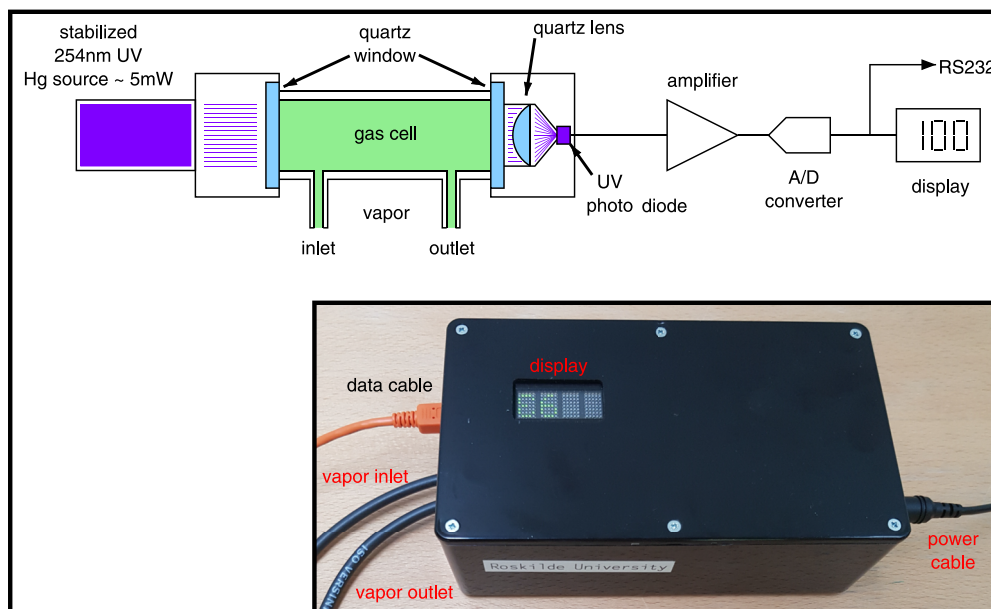


FIG. 3. Schematic overview of the *in situ* solvent vapor concentration (SVC) sensor. A/D and RS232 show the analog to digital converter and the data transfer protocol/cable from the SVC sensor to the computer, respectively. The inset in the bottom shows a photo of the SVC device.

where ϵ is the attenuation coefficient, l is the optical path length, and c is the concentration of attenuating species. The absorbance given in Eq. (2) is thus proportional to the concentration of solvent in the gas, i.e., the humidity of the gas, for a given species and fixed optical path length in the sensor.

III. RESULTS AND DISCUSSION

A. *In situ* optical film thickness measurement evaluation

The OFTM was evaluated using a two-layer (Si-substrate + Si-oxide) system, i.e., a standard Si-wafer (ID909, Ocean Optics Ltd.) developed for thickness calibration was used. The calibration wafer has SiO₂ oxide layers with differing thicknesses ranging from zero to 500 nm.⁴⁶ For probe assessment, the calibration wafer was used outside the STVA chamber in two different setups: (i) with the original commercial fiber before mounting the optics and window and (ii) with the fiber after mounting the optics and the MgF₂ coated sapphire window (see Fig. S5 and Table S1). The MgF₂ coated sapphire window is used due to the superiority in optical transmittance in the relevant wavelength region.⁴⁷ As seen in Table S1, for 100 nm and thicker films, the thicknesses measured with the two different setups do not differ significantly from the calibration value. Next, the thickness probe was evaluated using a three-layer system (i.e., Si-substrate + Si native oxide layer + polymer thin film) with the corresponding reference wafer. For this purpose, two polystyrene (molecular weight 50 kg/mole) homopolymer films were prepared by spin coating onto Si-wafers purchased from Topsil Co., Denmark (Fig. 4 and Table I)—nominal film thicknesses were ~100 and ~275 nm. By nominal thickness is referred to the expected film thickness resulting from the chosen polymer concentration and spin coating parameters

based on experience and thickness determination using a number of experimental techniques (e.g., ellipsometry and x-ray reflectivity). The actual film thicknesses are given in Table I and measured with optical reflectometry. The bare Topsil Si-wafer was used for the reference measurement. As seen from Fig. 4, the thicker film has more features in the reflectance curve than the thinner film, and hence, model fitting has smaller uncertainties in fitting parameters, the thicker the film. The dark signal is significantly increased after the addition of optics and window; this is seen in Fig. 4 when comparing Fig. 4(a) with Fig. 4(c) and Fig. 4(b) with Fig. 4(d). As a consequence, the difference between the total measured (reflected) intensity from the film and the dark reflected intensity alone is very small using optics and window. This is reflected in a higher level of noise in the reflectance curve. However, the reflectance curves calculated from Eq. (1) are overall very similar with and without optics and window for both film thicknesses, validating the use of the setup with optics and window despite a higher noise level. Accordingly, the thicknesses obtained from *in situ* measurements are in good agreement with measurements made using the fiber alone (see Table I).

B. *In situ* SVC sensor evaluation

During solvent vapor annealing, there is a flow of solvent through the STVA chamber. The exhaust gas is monitored by passing the exhaust through a home-build portable SVC sensor before the exhaust gas is finally let to a fume hood. To calibrate and evaluate the SVC sensor, a set of tests were performed (Fig. 5). For this purpose, a commercial UV-VIS detector (L-4250, from Hitachi, Japan) was connected to the chamber exhaust along with the SVC sensor. First, a steady state was introduced in the STVA chamber

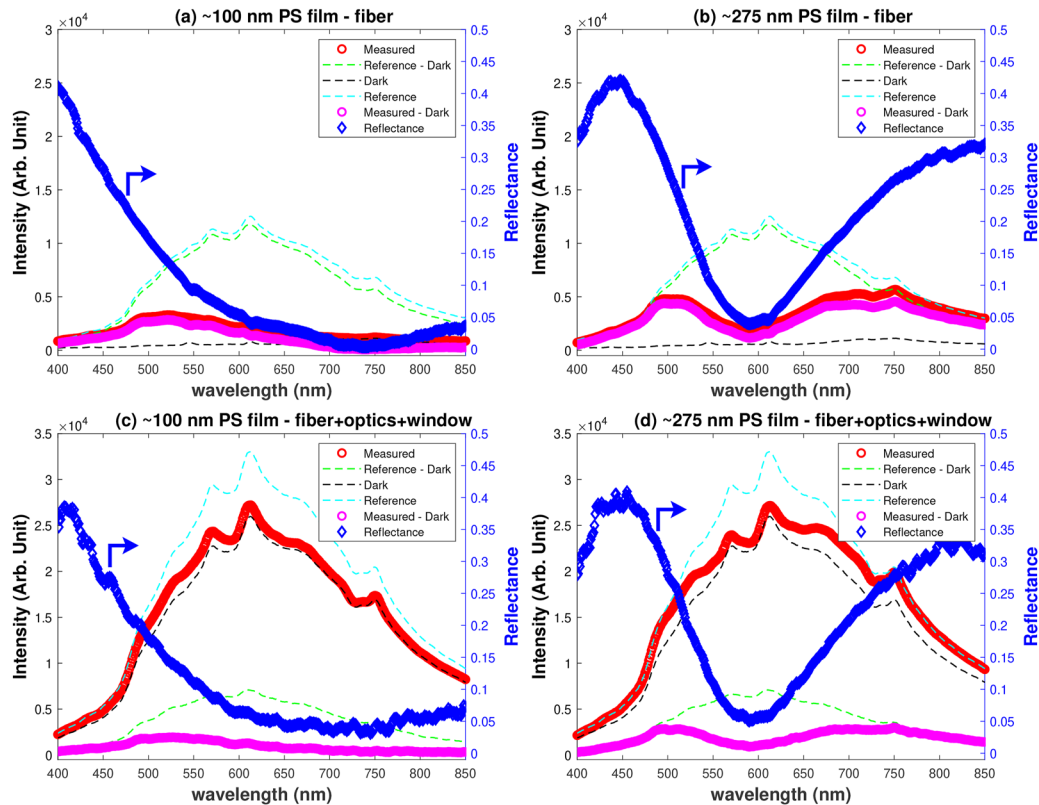


FIG. 4. Optical reflectometry results obtained from spin-coated polystyrene (PS) homopolymer films on Si-wafers with a native oxide layer. To the left, the ~ 100 nm thick PS film measured using the (a) fiber and (c) fiber + optics + MgF_2 coated sapphire window. To the right: the ~ 275 nm thick PS film measured with the (b) fiber and (d) fiber + optics + MgF_2 coated sapphire window. Red curves: Measured spectra, i.e. the overall intensity of the reflected light from the thin films, including stray light. Green dashed curves: Reference spectra measured from the bare wafer before spin coating with PS (the dark measurement is subtracted in this case). Black dashed curves: Dark spectra, i.e. the internally reflected light from the fiber/fiber + optics + MgF_2 coated sapphire window. Sky blue dashed curve: Reference spectra measured from the bare wafer before spin coating with PS. Pink curve: Overall intensity of reflected light from the thin film with dark measurement subtracted. Blue curves (right y axis): The resulting thin film reflectance curves obtained from Eq. (1).

with a flow of 100 sccm N_2 through the bubbler filled with solvent (in this case toluene). Then, the solvent vapor was purged from the chamber with 100 sccm dry N_2 . This way, the timescale for filling and emptying the STVA chamber with the relevant gas was determined. The SVC sensor data were compared to data obtained using the commercial spectrometer. Finally, data reproducibility tests were performed to evaluate how multiple consecutive chamber filling and

emptying cycles affect the SVC sensor data. The UV absorbance of the exhaust gas as a function of time (Fig. 5) was fitted with an exponential. The chamber volume is $\sim 375 \text{ cm}^3$, and the expected timescale for chamber filling/emptying is thus volume/(gas flow) $\sim 375 \text{ cm}^3 / (100 \text{ cm}_{\text{STP}}^3/\text{min}) \sim 225 \text{ s}$. The timescale for chamber filling (of a particular atmosphere, in casu toluene) was estimated from the data in Fig. 5 to be 229 and 236 s using, respectively, the SVC

TABLE I. OFTM results obtained *in situ* from spin-coated PS thin films with and without the optics and window included.

Film specification	Obtained thicknesses (nm)			
	With fiber		With fiber + optics + window	
	Si oxide	PS film	Si oxide	PS film
Si + Si native oxide layer + PS thin film	0.8	104	1.6	103
	1.0	278	1.0	278

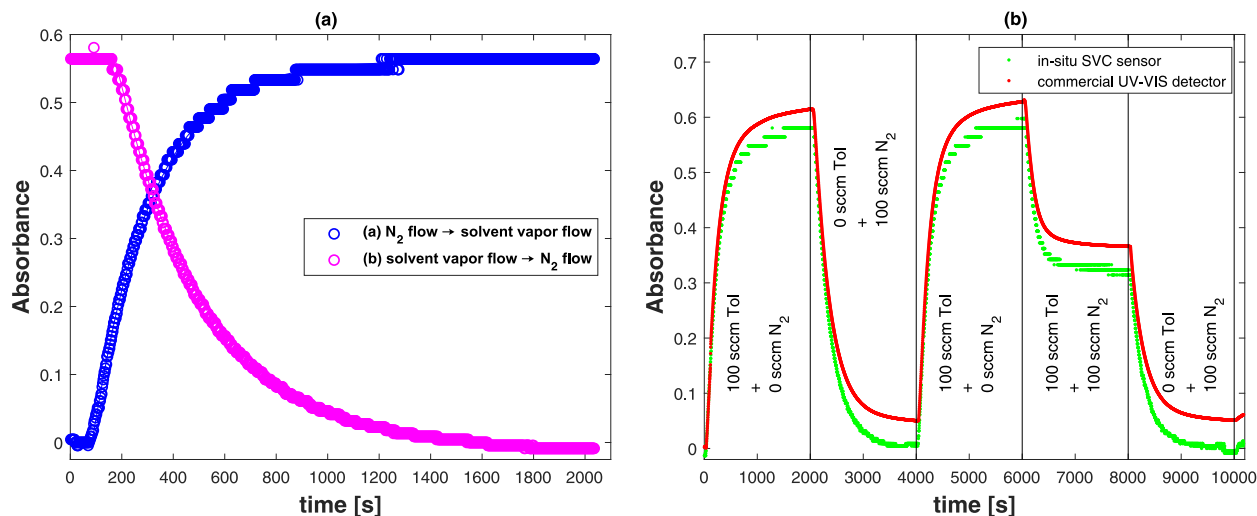


FIG. 5. Evaluation of the data obtained from the *in situ* SVC sensor, which is mounted to the exhaust of the STVA chamber: (a) the evaluation test during the exchange of the gas flow from dry to wet (i.e., 100 sccm pure N₂ flow → 100 sccm N₂ saturated with toluene vapor flow = chamber filling test) and vice versa (i.e., 100 sccm N₂ saturated with toluene vapor flow → 100 sccm pure N₂ flow = chamber emptying test) and (b) data reproducibility test along with the comparison between the *in situ* SVC sensor and the commercial UV-VIS detector.

sensor and the commercial spectrometer, i.e. consistent with the expected value. The timescale for chamber emptying (of a particular atmosphere, in casu toluene) was, respectively, 344 and 346 s for the SVC sensor and the commercial spectrometer, respectively, thus significantly higher than for filling. This is probably due to the presence of solvent “reservoirs” from condensation and adsorption to the interior walls of the tubing, solvent uptake in O-rings, etc. The longer timescale for filling using the commercial spectrometer was due to longer tube lengths since the SVC sensor was connected directly to the chamber exhaust, while the output from the SVC sensor was used as the input for the commercial spectro-

meter. According to Fig. 5(b), the data reproducibility during chamber filling and emptying was acceptable.

Figure 6 shows data for both toluene and acetone plotted as absorbance vs relative humidity, where the relative humidity is calculated as the ratio of solvent vapor flow (i.e., the N₂ flow passed through the bubbler assumed to be saturated with solvent vapor, i.e., 100% humidity) to the total flow from MFC/CEM channels,

$$\text{Humidity (gas wetness)} = \frac{\text{solvent vapor flow}}{(\text{N}_2 \text{ flow} + \text{solvent vapor flow})}. \quad (4)$$

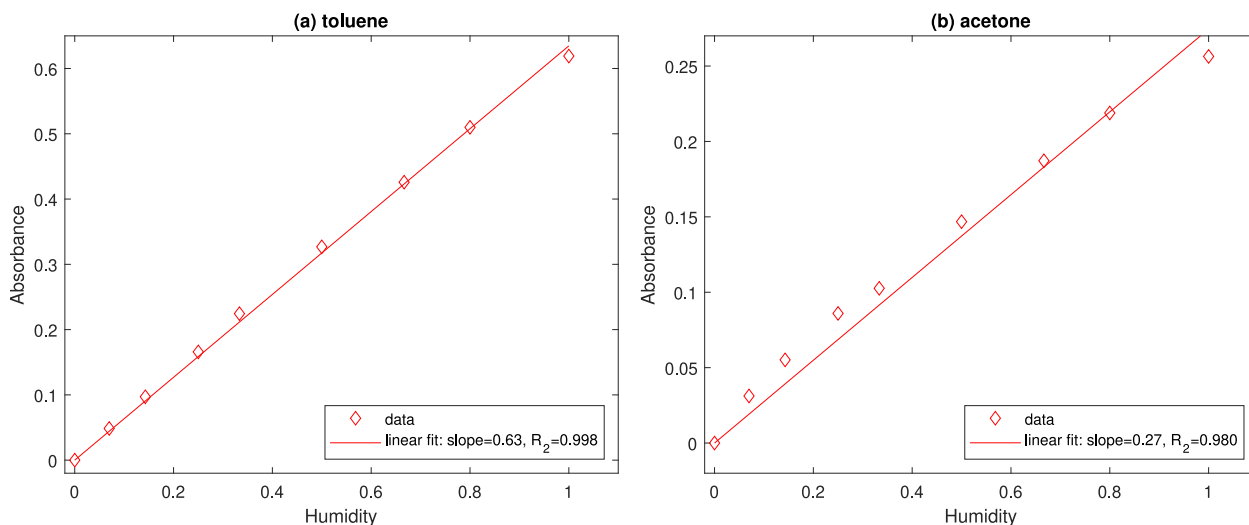


FIG. 6. SVC sensor absorbance as a function of humidity of exhaust gas for (a) toluene and (b) acetone as the solvent vapor in the exhaust gas.

The results show that the absorbance does indeed change linearly with the chamber humidity for both toluene and acetone (see Fig. 6). The differences of the slopes of the linear fits are due to toluene and acetone having different attenuation coefficients in the UV range (see the supplementary material).⁴⁴

C. Comparing solvent vapor delivery systems

In the combination of the MFC + bubbler, the solvent vapor flow is created by N₂ passing through the bubbler filled with liquid solvent. As mentioned above, it is assumed that N₂ bubbles are fully saturated with solvent vapor in the time it takes a N₂ bubble to pass through the liquid solvent. Using the combination of MFC and CEM, the solvent vapor flow is formed differently. A controlled stream of liquid solvent is mixed with the appropriate gas flow from a MFC followed by evaporation of the liquid part of the mixture at the relevant temperature in the CEM unit. To compare the methods, experiments were performed using comparable flow scripts with the MFC + bubbler and with the MFC + CEM (Fig. 7). The SVC was used to measure the exhaust gas composition created by the two methods. For the STVA runs performed with the MFC + CEM, all FLUIDAT calculations are performed at the chosen STVA chamber temperature, but the actual temperature of the CEM evaporator is set 3–5 °C higher than the value used in the calculations. This was done in order to compensate for any temperature drops from the CEM unit to the STVA chamber and hence minimize the risk of solvent vapor condensation in the tubing connecting the CEM to the STVA chamber. When the gas enters the mixing box integrated in the STVA chamber wall, it is thermalized to the desired temperature and, hence, has the desired humidity when entering the STVA chamber. As can be seen in Fig. 7, the chamber atmosphere formed with the two different solvent vapor delivery sub-systems is comparable judged by the solvent vapor content in the exhaust, i.e., the absorbance. Likewise, the timescales for the output response to changes in the sub-system inputs to the STVA chamber are very

similar. Especially for large humidity values, the bubbler data have somewhat lower absorbance of the exhaust gas, i.e., the assumption of 100% humidity for the N₂ gas passing through the bubbler might be too optimistic.

Solvent vapor annealing is a highly versatile annealing technique, and using two solvents opens a wealth of possibilities for controlling block copolymer structuring using, e.g., a selective and non-selective solvent.⁴⁸ The system design presented here is prepared for using two solvents. This can be done in different ways, using either two bubblers, using the bubbler and the CEM or using a solvent mixture in the CEM.

D. Test measurements on homopolymer thin films

The STVA setup was tested by swelling thin homopolymer films spin coated onto Si wafers: ~100 nm thick polyisoprene (PI) and ~100 nm thick polystyrene (PS) films were swollen with acetone and toluene, respectively (see Fig. 8). All measurements were performed at room temperature where PS is a glass (i.e., below the glass transition), while PI is a rubber (above the glass transition); however, uptake of solvent will eventually shift the glass transition temperature such that PS for high SRs has crossed the glass transition. From the Fox equation, it is estimated that T_g for PS will reach room temperature for a swelling ratio of 1.18 when swelling with toluene and 1.16 when swelling with acetone.^{49,50} This estimation is disregarding any thickness induced decrease of T_g , which is not significant for a 100 nm thick PS film.⁵¹ For all four cases investigated, changes in the solvent content of the exhaust gas as measured by the SVC sensor and changes in the film thickness/swelling ratio are to a large degree synchronized stepwise. However, for low SRs, especially the swelling of the glassy PS film does not synchronize to the stepwise increase in humidity, but has a more smooth time dependence. Whether a solvent is a good or a bad solvent for a given polymer is tabulated in terms of the Hildebrand solubility parameter, δ , which is the square root of the cohesive energy density.⁵² Materials with

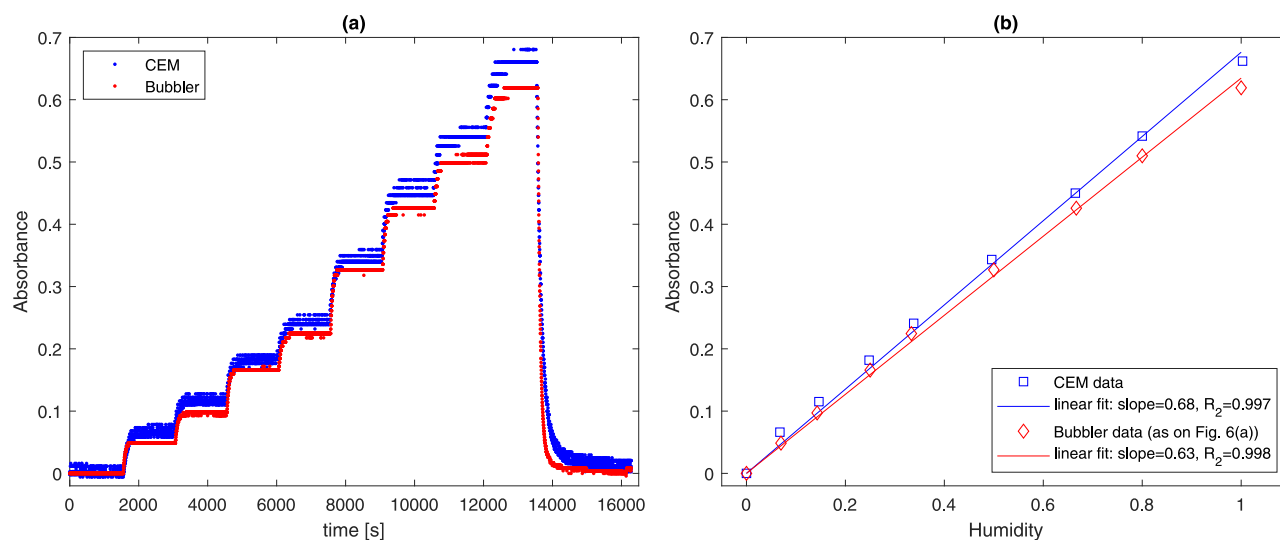


FIG. 7. Comparing solvent vapor delivery systems, i.e., the combination of MFC and bubbler vs the combination of MFC and CEM: (a) SVC absorbance vs time for the two delivery systems using toluene as solvent. (b) SVC absorbance vs gas humidity as defined in Eq. (4) for the two delivery systems.

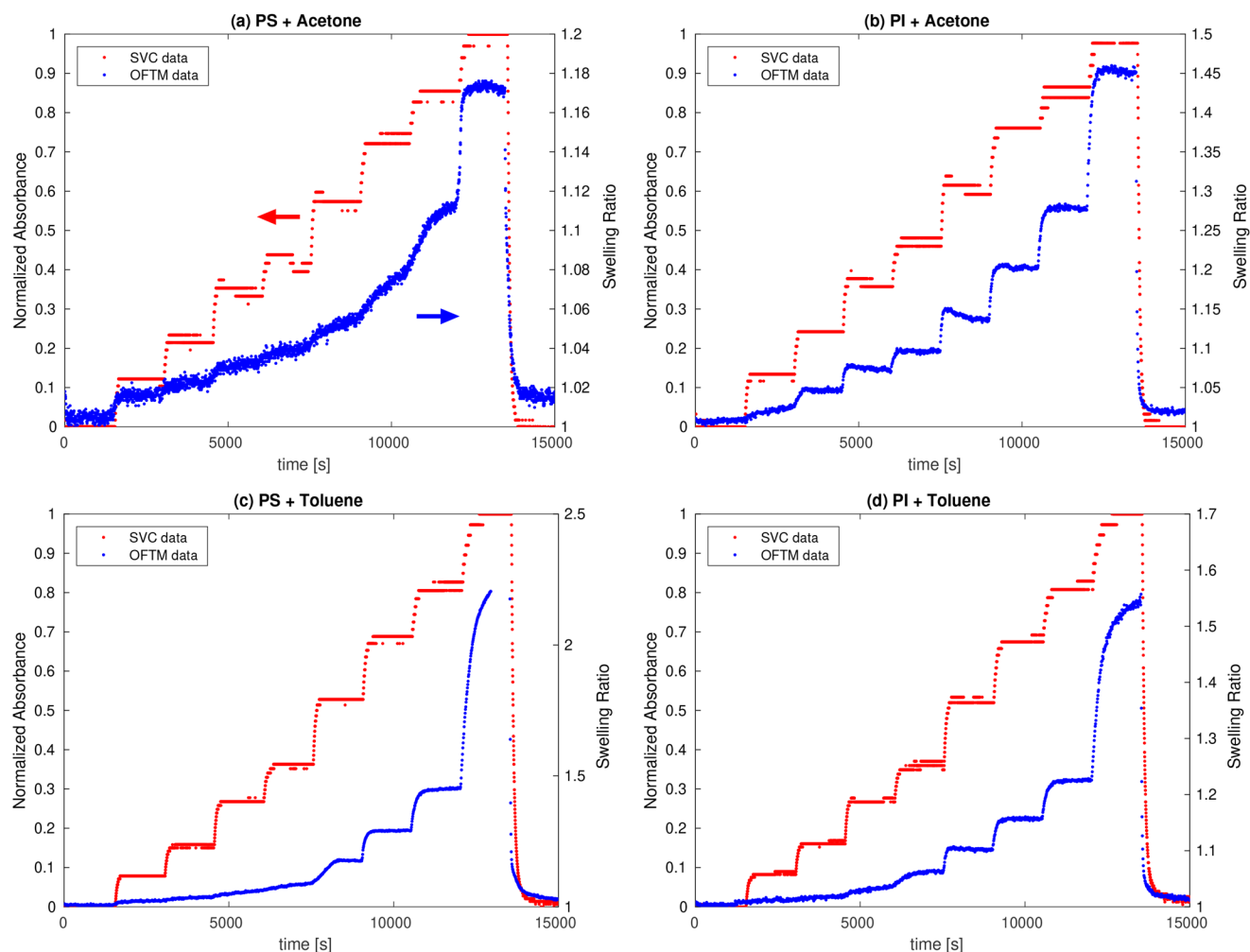


FIG. 8. Swelling behavior of PS and PI thin films under (a) and (b) acetone and under (c) and (d) toluene vapor. Red data, left axis: SVC data, i.e., UV absorbance in the exhaust gas (normalized to maximum value 1); blue data, right axis: *in situ* OFTM thickness data, $h(t)$, presented as the swelling ratio, $SR = h(t)/h_0$.

similar values of δ are likely to be miscible. The values for the Hildebrand solubility parameter for the four relevant materials in this investigation are: polyisoprene $\delta_{PI} = 8.2$ (cal/cm³)^{1/2}, polystyrene $\delta_{PS} = 8.7$ (cal/cm³)^{1/2}, toluene $\delta_{Toluene} = 8.9$ (cal/cm³)^{1/2}, and acetone $\delta_{Acetone} = 9.9$ (cal/cm³)^{1/2}.⁵² According to these values, both PI and PS are more soluble in toluene than in acetone, the best match (in terms of solubility) being PS and toluene. At 100% chamber humidity, the maximum swelling ratio, SR_{max} , for PS is ~ 2.3 in toluene and ~ 1.2 in acetone vapor, which is consistent with the δ values. Likewise, SR_{max} for PI is ~ 1.6 in toluene and ~ 1.5 in acetone. Comparing to the relevant δ -value differences, i.e., $\Delta\delta_{PS-toluene} < \Delta\delta_{PI-toluene} < \Delta\delta_{PS-acetone} < \Delta\delta_{PI-acetone}$, it is expected that $SR_{PS-toluene} > SR_{PI-toluene} > SR_{PS-acetone} > SR_{PI-acetone}$ would be the outcome of film swelling experiments. This is also what is observed, apart from the low degree of swelling of PS with acetone, which might be related to PS still being in the glassy state. In all four cases, the last step up in humidity is accompanied by a very large step in swelling ratio, the mechanism

behind this observation not being fully understood yet and thus needing more investigations. The behavior might be related to a “kink” in the sorption curve (solvent volume fraction in film vs solvent activity) observed previously for, e.g., thin films of PS brushes swollen with toluene.⁵³

IV. CONCLUSION

A compact STVA setup is presented, which compared to previous similar setups has improved performance with respect to condensation in tubes and enclosures. For monitoring the STVA process *in situ*, the setup is equipped with a commercial film thickness measuring device (optical reflectometry) and a home-build solvent vapor concentration sensor (UV absorption) monitoring the amount of organic solvent in the chamber exhaust. Two different solvent vapor delivery systems were tested: (a) a bubbler with a liquid solvent reservoir where dry N₂ gas is saturated with solvent

vapor when passing through the bubbler (the solvent humidity of the gas exiting the bubbler did in certain cases not quite reach 100%) and (b) a commercial CEM system where liquid solvent and N₂ gas are mixed and transferred to an evaporator before the resulting gas mixtures having a well-defined solvent partial pressure and temperature are let into the STVA chamber at a well-defined flow rate. Both systems successfully allow for a change of the atmosphere in the STVA chamber from dry (100% N₂ flow) to wet (i.e., 0%–100% solvent humidity) and vice versa with time-constants of a few hundred seconds. The setup is thermally well isolated from the surroundings, and the absolute precision of the chamber temperature is ± 1 K.

The setup presented has successfully been shipped to and used at different international synchrotron facilities for GISAXS experiments with different solvents in the temperature range from room temperature to 50 °C.⁵⁴ When raising the temperature, it is important to be aware of the boiling point of the solvent used for annealing. Apart from this consideration, there are no fundamental limitations for going even higher in temperature, e.g., 60–70 °C, but in this range, attention has to be paid to softening of glue and sensitivity of other components to long term exposure to hot solvent gas. Especially when using the bubbler system, measurements should be performed well below the boiling point of the solvent in question. Current work in progress aims at decreasing the STVA chamber volume for faster humidity changing times and at improving the routine for exchange of samples together with improved robust OFTM fiber coupling to the STVA chamber working also under harsh conditions. A SVC sensor with temperature control and improved stability is also under construction. The setup has been used for *in situ* swelling and annealing studies of block copolymer and polymer films, but will also find use for studies of, e.g., biological relevant samples in a humidity and temperature-controlled atmosphere.

SUPPLEMENTARY MATERIAL

See the supplementary material for photos of the setup, a schematic figure showing the layer models used to fit OFTM data together with OFTM data for the calibration Si-wafer, and UV absorbance spectra for toluene and acetone.

ACKNOWLEDGMENTS

Support by the Danish National Research Foundation, Project DFF—Grant No. 7014-00288 (filmSTAR), to D.P. and S.A. is gratefully acknowledged. Detlef-M. Smilgies and CHESS, Cornell University, are thanked for access to perform *in situ* GISAXS experiments using our equipment. Ebbe Hyldahl Larsen and Bjarne Christensen from the INM/RUC workshop are thanked for expert technical assistance. Jonathan Michael Gow, RUC, is thanked for software for optical reflectometry model calculations.

AUTHOR DECLARATIONS

Conflict of Interest

The authors have no conflicts to disclose.

Author Contributions

Sina Ariaee: Data curation (equal); Investigation (equal); Visualization (lead); Writing – original draft (lead); Writing – review & editing (supporting). **Bo Jakobsen:** Methodology (lead); Software (lead); Writing – review & editing (supporting). **Ib Høst Pedersen:** Data curation (equal); Investigation (equal); Methodology (equal). **Torben Steen Rasmussen:** Methodology (equal). **Dorthe Posselt:** Conceptualization (lead); Funding acquisition (lead); Project administration (lead); Supervision (lead); Writing – review & editing (lead).

DATA AVAILABILITY

The data that support the findings of this study are available from the corresponding author upon reasonable request.

REFERENCES

- D. T. Hoang, J. Yang, K. Paeng, Y. Kwon, O. S. Kweon, and L. J. Kaufman, *Rev. Sci. Instrum.* **87**(1), 015106 (2016).
- F. Müller-Plathe, *Macromolecules* **29**(13), 4782–4791 (1996).
- T. S. Chow, *Macromolecules* **13**(2), 362–364 (1980).
- C. M. Bates and F. S. Bates, *Macromolecules* **50**(1), 3–22 (2017).
- H. Hultkonen, T. Salminen, and T. Niemi, *Soft Matter* **15**(39), 7909–7917 (2019).
- Y. J. Choi, M. H. Byun, T. W. Park, S. Choi, J. Bang, H. Jung, J.-H. Cho, S.-H. Kwon, K. H. Kim, and W. I. Park, *ACS Appl. Nano Mater.* **2**(3), 1294–1301 (2019).
- C. Jin, B. C. Olsen, E. J. Luber, and J. M. Buriak, *Chem. Mater.* **29**(1), 176–188 (2017).
- C. Cummins, T. Ghoshal, J. D. Holmes, and M. A. Morris, *Adv. Mater.* **28**(27), 5586–5618 (2016).
- R. Lundy, S. P. Flynn, C. Cummins, S. M. Kelleher, M. N. Collins, E. Dalton, S. Daniels, M. A. Morris, and R. Enright, *Phys. Chem. Chem. Phys.* **19**(4), 2805–2815 (2017).
- S. P. Nunes, *Sustainable Nanoscale Engineering*, edited by G. Szekely and A. Livingston (Elsevier, 2020), pp. 297–316.
- M. Babics, R.-Z. Liang, K. Wang, F. Cruciani, Z. Kan, M. Wohlfahrt, M.-C. Tang, F. Laquai, and P. M. Beaujuge, *Chem. Mater.* **30**(3), 789–798 (2018).
- A. M. Barnes, Y. Du, W. Zhang, S. Seifert, S. K. Buratto, and E. B. Coughlin, *Macromolecules* **52**(16), 6097–6106 (2019).
- D. Posselt, J. Zhang, D.-M. Smilgies, A. V. Berezkin, I. I. Potemkin, and C. M. Papadakis, *Prog. Polym. Sci.* **66**, 80–115 (2017).
- P. Mansky, P. haikin, and E. L. Thomas, *J. Mater. Sci.* **30**(8), 1987–1992 (1995).
- C. Sinturel, M. Vayer, M. Morris, and M. A. Hillmyer, *Macromolecules* **46**(14), 5399–5415 (2013).
- G. De Luca, E. Treossi, A. Liscio, J. M. Mativetsky, L. M. Scolaro, V. Palermo, and P. Samori, *J. Mater. Chem.* **20**(13), 2493–2498 (2010).
- J. Arias-Zapata, S. Böhme, J. Garnier, C. Girardot, A. Legrain, and M. Zelsmann, *Adv. Funct. Mater.* **26**(31), 5690–5700 (2016).
- L. Tsarkova, *Macromolecules* **45**(19), 7985–7994 (2012).
- S. H. Kim, M. J. Misner, T. Xu, M. Kimura, and T. P. Russell, *Adv. Mater.* **16**, 226–231 (2004).
- Z. Di, D. Posselt, D.-M. Smilgies, and C. M. Papadakis, *Macromolecules* **43**(1), 418–427 (2010).
- M. Luo and T. H. Epps, *Macromolecules* **46**(19), 7567–7579 (2013).
- M. Vayer, M. A. Hillmyer, M. Dirany, G. Thevenin, R. Erre, and C. Sinturel, *Thin Solid Films* **518**, 3710–3715 (2010).
- Y. S. Jung and C. A. Ross, *Adv. Mater.* **21**(24), 2540–2545 (2009).
- S. S. Dinachali, W. Bai, K.-H. Tu, H. K. Choi, J. Zhang, M. E. Kreider, L.-C. Cheng, and C. A. Ross, *ACS Macro Lett.* **4**(5), 500–504 (2015).
- G. Nelson, C. S. Drapes, M. A. Grant, R. Gnabasiak, J. Wong, and A. Baruth, *Micromachines* **9**(6), 271 (2018).

- ²⁶K. W. Gotrik, A. F. Hannon, J. G. Son, B. Keller, A. Alexander-Katz, and C. A. Ross, *ACS Nano* **6**(9), 8052–8059 (2012).
- ²⁷A. Knoll, R. Magerle, and G. Krausch, *J. Chem. Phys.* **120**(2), 1105–1116 (2004).
- ²⁸S. Park, X. Cheng, A. Böker, and L. Tsarkova, *Adv. Mater.* **28**(32), 6900–6905 (2016).
- ²⁹M. Y. Efremov and P. F. Nealey, *Rev. Sci. Instrum.* **89**(5), 055114 (2018).
- ³⁰K. W. Gotrik and C. A. Ross, *Nano Lett.* **13**(11), 5117–5122 (2013).
- ³¹J. M. Kim, Y. Kim, W. I. Park, Y. H. Hur, J. W. Jeong, D. M. Sim, K. M. Baek, J. H. Lee, M.-J. Kim, and Y. S. Jung, *Adv. Funct. Mater.* **25**(2), 306–315 (2015).
- ³²S. Kim, G. Jeon, S. W. Heo, H. J. Kim, S. B. Kim, T. Chang, and J. K. Kim, *Soft Matter* **9**(23), 5550–5556 (2013).
- ³³J. Yin, X. Yao, J.-Y. Liou, W. Sun, Y.-S. Sun, and Y. Wang, *ACS Nano* **7**(11), 9961–9974 (2013).
- ³⁴X. Cheng, A. Böker, and L. Tsarkova, *Polymers* **11**(8), 1312 (2019).
- ³⁵M. J. Kim, W. I. Park, Y. J. Choi, Y. K. Jung, and K. H. Kim, *RSC Adv.* **6**(25), 21105–21110 (2016).
- ³⁶E. Kim, H. Ahn, S. Park, H. Lee, M. Lee, S. Lee, T. Kim, E.-A. Kwak, J. H. Lee, X. Lei, J. Huh, J. Bang, B. Lee, and D. Y. Ryu, *ACS Nano* **7**(3), 1952–1960 (2013).
- ³⁷K. Kim, S. Park, Y. Kim, J. Bang, C. Park, and D. Y. Ryu, *Macromolecules* **49**(5), 1722–1730 (2016).
- ³⁸Y.-C. Huang, H.-C. Chia, C.-M. Chuang, C.-S. Tsao, C.-Y. Chen, and W.-F. Su, *Sol. Energy Mater. Sol. Cells* **114**, 24–30 (2013).
- ³⁹J. E. Maslar, W. A. Kimes, B. A. Sperling, and R. K. Kanjolia, *J. Vac. Sci. Technol. A* **37**(4), 041506 (2019).
- ⁴⁰A. V. Berezkin, F. Jung, D. Posselt, D. M. Smilgies, and C. M. Papadakis, *Adv. Funct. Mater.* **28**(19), 1706226 (2018).
- ⁴¹A. Stenbock-Fermor, A. W. Knoll, A. Böker, and L. Tsarkova, *Macromolecules* **47**(9), 3059–3067 (2014).
- ⁴²C. K. Shelton and T. H. Epps, *Macromolecules* **49**(2), 574–580 (2016).
- ⁴³M. J. Maher, J. L. Self, P. Stasiak, G. Blachut, C. J. Ellison, M. W. Matsen, C. M. Bates, and C. G. Willson, *ACS Nano* **10**(11), 10152–10160 (2016).
- ⁴⁴T. G. Mayerhöfer and J. Popp, “Beer’s law – Why absorbance depends (almost) linearly on concentration,” *ChemPhysChem* **20**(4), 511–515 (2019).
- ⁴⁵Beer, *Ann. Phys.* **162**(5), 78–88 (1852).
- ⁴⁶H. R. Huff, U. Gösele, H. Tsuya, and N. J. Pennington, “Silicon materials science and technology,” in *Proceedings of the 18th International Symposium on Silicon Materials Science and Technology* (Pennington, NJ, 1998).
- ⁴⁷K. Marszałek, P. Winkowski, and M. Marszałek, *Mater. Science-Poland* **33**(1), 6–10 (2015).
- ⁴⁸F. A. Jung, A. V. Berezkin, T. B. Tejsner, D. Posselt, D. M. Smilgies, and C. M. Papadakis, *Macromol. Rapid Commun.* **41**(14), 2000150 (2020).
- ⁴⁹J. Zhang, D. Posselt, D.-M. Smilgies, J. Perlich, K. Kyriakos, S. Jaksch, and C. M. Papadakis, *Macromolecules* **47**(16), 5711–5718 (2014).
- ⁵⁰T. G. Fox and S. Loshaek, *J. Polym. Sci.* **15**(80), 371–390 (1955).
- ⁵¹J. L. Keddie, R. A. L. Jones, and R. A. Cory, *Europhys. Lett.* **27**(1), 59 (1994).
- ⁵²J. Brandrup, E. H. Immergut, E. A. Grulke, A. Abe, and D. R. Bloch, *Polymer Handbook* (Wiley, New York, 1999).
- ⁵³A. Laschitsch, C. Bouchard, J. Habicht, M. Schimmel, J. Rühe, and D. Johannsmann, *Macromolecules* **32**(4), 1244–1251 (1999).
- ⁵⁴F. A. Jung, D. Posselt, D.-M. Smilgies, P. A. Panteli, C. Tsitsilianis, C. S. Patrickios, and C. M. Papadakis, *Macromolecules* **53**(15), 6255–6266 (2020).